Investigation of Boundary Algorithms for Multiresolution Analysis

Martin Peschke and Wolfgang Menzel, *Fellow, IEEE*

***Abstract*—An investigation on the multiresolution time-domain (MRTD) method utilizing different wavelet levels in one mesh is presented. Contrary to adaptive thresholding techniques, only a rigid addition of higher order wavelets in certain critical cells is considered. Their effect is discussed analytically and verified by simulations of plain and dielectrically filled cavities with Daubechies' and Battle–Lemarie orthogonal, as well as Cohen–Daubechies–Feauveau (CDF) biorthogonal wavelets, showing their insufficiency unless used as a full set of expansion. It is pointed out that improvements cannot be expected from these fixed mesh refinements. Furthermore, an advanced treatment concerning thin metallization layers in CDF algorithms is presented, leading to a reduction in cell number by a factor of three per space dimension compared to conventional finite difference time domain (FDTD), but limited to very special structures with infinitely thin irises. All MRTD results are compared to those of conventional FDTD approaches.**

***Index Terms*—Boundary conditions, multiresolution analysis, time-domain methods, wavelets.**

I. Introduction

THE multiresolution time-domain (MRTD) method has been under examination by various publications in the past. This includes the wavelet Galerkin scheme based on Battle–Lemarie [1], Haar [2], Daubechies orthogonal ([3], slightly different algorithm) and Cohen–Daubechies–Feauveau (CDF) biorthogonal wavelets [4]. In structures with mainly harmonic spatial field distribution, it was shown analytically and by several simulations that the new approach reduces the numerical phase error drastically, allowing a reduced cell number by up to two orders of magnitude.

Additionally, all prementioned authors claim that MRTD achieves a natural mesh refinement such as introducing denser discretization rates for field components with fast spatial variation by adding wavelets of higher order. This feature is expected to further reduce the numerical effort and to contribute to an exact localization of different boundary conditions [5]. Thus far, the only publication dealing with an *a priori* mesh refinement is [6], but results are compared only qualitatively to those of finite difference time domain (FDTD) with a very high discretization rate. If any, this paper's analytical survey and computational validation indicates that an advantage of such approaches cannot be expected in general. At last, dynamical mesh adaption remains a possibility for enhancing MRTD's performance ([3], [7]).

Another often applied approach is the FDTD-like treatment of dielectric boundaries by local sampling for Daubechies or CDF wavelets in scaling functions only [8], neglecting the exact material operator that has to actually be deployed. It will be shown that, even with one-dimensional cavities, this simplified algorithm yields worse results compared to conventional FDTD.

MRTD's speed can be improved by pre-calculating boundary field dependencies (Massachusetts Institute of Technology (MIT), Cambridge, technique, [9]), but this approach does not affect accurateness and is very memory expensive for large calculation areas and arbitrary structures.

Finally, all but concave edges represent a problem for wavelet schemes incorporating an image principle to model perfect electric boundaries, explaining their rare appearance in most publications thus far. This paper presents a new treatment for thin metallic irises by CDF algorithms.

II. MRTD Formulation

The (biorthogonal) wavelet representation of propagating fields, for simplicity in one dimension only, but for an arbitrary order of expansion, is as follows:

$$E_x(y,t) = \sum_k \sum_m \sum_q E_{x\,m}^{\,q}(k) \cdot \tilde{\Psi}_m^q(y) \cdot h_k(t) \tag{1}$$

$$H_z(y,t) = \sum_k \sum_m \sum_q H_{z\,q}^{\,m}(k) \cdot \tilde{\Psi}_{m+1/2}^{\,q}(y) \cdot h_{k+(1/2)}(t). \tag{2}$$

$\tilde{\Psi}_m^q(y)$ is a dual-wavelet function of order q displaced by m units Δy, and $h_k(t)$ is the zeroth-order rectangular Haar wavelet shifted by k units Δt in time [4]. For orthogonal wavelet bases like the Battle–Lemarie and Haar family, $\tilde{\Psi}_m^q(y)$ equals $\Psi_m^q(y)$.

Extension to the three-dimensional case is straightforward, replacing coefficients E, $H_{\nu\,m}^{\,q}(k)$ by E, $H_{\nu\,lmn}^{\,pqr}(k)$, and all components shifted according to the Yee scheme like in [1], e.g.,

$$E_x(\vec{r},t) = \sum_k \sum_{l,m,n} \sum_{p,q,r} E_{x\,lmn}^{\,pqr}(k) \tilde{\Psi}_{l+(1/2)}^{p}(x) \tilde{\Psi}_m^q(y) \times \tilde{\Psi}_n^r(z) h_k(t). \tag{3}$$

The letters l, m, and n indicate the Yee cell number in three dimensions, p, q, and r the according wavelet level, respectively.

Manuscript received September 9, 2002; revised October 31, 20002.

M. Peschke is with the Department of Optoelectronics, University of Ulm, D-89069 Ulm, Germany (e-mail: peschke_martin@hotmail.com).

W. Menzel is with Microwave Techniques, University of Ulm, D-89069 Ulm, Germany (e-mail: wolfgang.menzel@ieee.org).

Digital Object Identifier 10.1109/TMTT.2003.809666

TABLE I
CONNECTION COEFFICIENTS FOR HAAR WAVELETS

p	0		1	
$\tilde{p}$	0	1	0	1
i				
-1	-1	0	0	-1
0	$+1$	0	0	$+1$

TABLE II
CONNECTION COEFFICIENTS FOR CDF$(2,2)$ WAVELETS

p	0		1	
$\tilde{p}$	0	1	0	1
i				
-1	-1.2291667	0	$+0.0416667$	-1.4375000
0	$+1.2291667$	-0.1510417	0	$+1.4375000$
$+1$	-0.0937500	$+0.0833333$	-0.0416667	$+0.0937500$
$+2$	$+0.0104167$	-0.0052083	$+0.0208333$	-0.0104167

TABLE III
CONNECTION COEFFICIENTS FOR BATTLE–LEMARIE WAVELETS

p	0		1	
$\tilde{p}$	0	1	0	1
i				
-1	-1.2918462	0	$+0.0465973$	-2.4725388
0	$+1.2918462$	-0.0465973	0	$+2.4725388$
$+1$	-0.1560761	$+0.0545394$	-0.0465973	$+0.9562282$
$+2$	$+0.0596391$	-0.0369996	$+0.0545394$	$+0.1660587$
$+3$	-0.0293099	$+0.0205745$	-0.0369996	$+0.0939244$
$+4$	$+0.0153716$	-0.0111530	$+0.0205745$	$+0.0031413$
$+5$	-0.0081892	$+0.0059769$	-0.0111530	$+0.0134936$
$+6$	$+0.0043788$	-0.0032026	$+0.0059769$	-0.0028589
$+7$	-0.0023433	$+0.0017141$	-0.0032026	$+0.0027788$
$+8$	$+0.0012542$	-0.0009177	$+0.0017141$	-0.0011295

Introducing the field expansion into Maxwell's equations, the update instructions for the one-dimensional case are derived by testing with the nondual wavelet functions $\Psi_m^q(y)$

$$E_{x_m}^{\ q}(k+1) = E_{x_q}^{\ m}(k) + \frac{\Delta t}{\varepsilon \Delta y} \sum_{\tilde{m}} \sum_{\tilde{q}} a(\tilde{m}-m, q, \tilde{q}) \cdot H_{z_{\tilde{m}}}^{\tilde{q}}(k) \tag{4}$$

$$H_{z_q}^{\ m}(k+1) = H_{z_m}^{\ q}(k) + \frac{\Delta t}{\mu \Delta y} \sum_{\tilde{m}} \sum_{\tilde{q}} a(\tilde{m}-m-1, q, \tilde{q}) \cdot E_{x_{\tilde{m}}}^{\tilde{q}}(k+1) \tag{5}$$

with the connection coefficient

$$a(i,q,\tilde{q}) := \int_{-\infty}^{\infty} \frac{d}{dy} \tilde{\Psi}_{i+(1/2)}^{\tilde{q}}(y) \cdot \Psi_0^q(y) dy. \tag{6}$$

Numerical values up to the first order are given in Tables I–III for recently used wavelet families with the symmetry relationship $a(-i,0,0) = -a(i-1,0,0)$, $a(-i,0,1) = -a(i-2,0,1)$, $a(-i,1,0) = -a(i,1,0)$, and $a(-i,1,1) = -a(i-1,1,1)$. Recently, [6] presented a way of calculating the connection coefficients directly out of wavelet's filter coefficients.

III. ANALYTICAL ANALYSIS

A. Homogeneous Formulations

Analytical investigations on MRTD's dispersion properties have been done by [4] and [10]. However, only homogeneous expansions of zeroth or first order across the whole calculation area have been considered, and spurious solutions are neglected. According to the formulation in [10], first-order fields are arranged as follows:

$$Ex_m^0(k) = \underline{E}_0 \cdot e^{j(\beta_n m \Delta y - \omega k \Delta t)} \tag{7}$$

$$E_{x_m}^{\ 1}(k) = \underline{E}_1 \cdot e^{j(\beta_n (m+1/2) \Delta y - \omega k \Delta t)} \tag{8}$$

$$H_{z_m}^0(k) = \underline{H}_0 \cdot e^{j(\beta_n (m+1/2) \Delta y - \omega (k+1/2) \Delta t)} \tag{9}$$

$$H_{z_m}^{\ 1}(k) = \underline{H}_1 \cdot e^{j(\beta_n (m+1) \Delta y - \omega (k+1/2) \Delta t)}. \tag{10}$$

$\beta_n = 2\pi/\lambda_n$ denotes the numerical wavenumber in coefficient space, which differs from the real case $\beta = 2\pi/\lambda$ for a fixed angle frequency ω. By introducing (7)–(10) and after some mathematical manipulations, the update (4) and (5) yield an eigenvalue problem for the plane-wave amplitudes $\underline{E}_0$ to $\underline{H}_1$ after some mathematical operations as follows:

$$\begin{pmatrix} \underline{E}_0 \\ \underline{E}_1 \\ \underline{H}_0 \\ \underline{H}_1 \end{pmatrix} = \underbrace{- \begin{pmatrix} 0 & 0 & \frac{C_{00}}{Z_F} & \frac{C_{01}}{Z_F} \\ 0 & 0 & \frac{C_{10}}{Z_F} & \frac{C_{11}}{Z_F} \\ C_{00} Z_F & C_{01} Z_F & 0 & 0 \\ C_{10} Z_F & C_{11} Z_F & 0 & 0 \end{pmatrix}}_{C} \begin{pmatrix} \underline{E}_0 \\ \underline{E}_1 \\ \underline{H}_0 \\ \underline{H}_1 \end{pmatrix} \tag{11}$$

$$C_{00} = \hat{q} \cdot \frac{\sum_i a(i,0,0) \cdot \sin\left(\frac{\pi u (2i+1)}{n_l}\right)}{\sin\left(\frac{\pi \hat{q}}{n_l}\right)} \tag{12}$$

$$C_{01} = \hat{q} \cdot \frac{\sum_i a(i,0,1) \cdot \sin\left(\frac{\pi u (2i+2)}{n_l}\right)}{\sin\left(\frac{\pi \hat{q}}{n_l}\right)} \tag{13}$$

$$C_{10} = \hat{q} \cdot \frac{\sum_i a(i,1,0) \cdot \sin\left(\frac{\pi u (2i)}{n_l}\right)}{\sin\left(\frac{\pi \hat{q}}{n_l}\right)} \tag{14}$$

$$C_{11} = \hat{q} \cdot \frac{\sum_i a(i,1,1) \cdot \sin\left(\frac{\pi u (2i+1)}{n_l}\right)}{\sin\left(\frac{\pi \hat{q}}{n_l}\right)}. \tag{15}$$

The matrix elements C_{ij} are the connecting terms between the orders i and j, $\hat{q} := c_0 \Delta t / \Delta y$ is the Courant number, $u := \lambda/\lambda_n$ is the ratio between real and numerical wavelength, $n_l := \lambda/\Delta y$ is the number of Yee cells per wavelength, and Z_F is the free-space wave impedance. The dispersion relationship is obtained from $\det(\boldsymbol{C} - \boldsymbol{I}) = 0$ as follows:

$$1 - C_{00}^2 - C_{11}^2 - 2C_{01}C_{10} + (C_{00}C_{11} - C_{01}C_{10})^2 = 0. \tag{16}$$

This is almost the same result as in [4], where the factor 2 in front of the forth term obviously has been forgotten.

Fig. 1 compares the implicit equation (16) in the form of a wavelength error over discretization rate for CDF$(2,2)$ wavelets with the zeroth-order solution $1 - C_{00}^2 = 0$. Like for the Battle–Lemarie family, a spurious branch is obtained in addition to the improved curve.

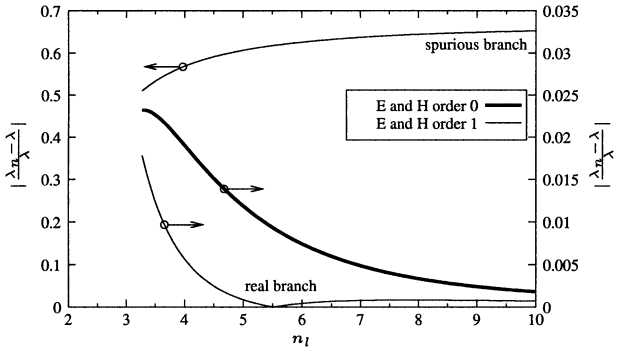

Fig. 1. Dispersion properties of complete zeroth- and first-order approaches using $\mathrm{CDF}(2,2)$ wavelets. The Courant number is $\hat{q} = 0.25$. The numerical wavelength error is plotted versus the number of cells per wavelength for wavelets of order 0 and 1.

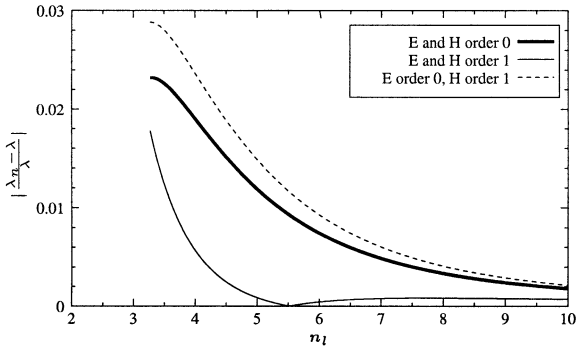

Fig. 2. Dispersion properties of the multiresolution approach using $\mathrm{CDF}(2,2)$ wavelets. The Courant number is $\hat{q} = 0.25$. As in Fig. 1, the plot shows the numerical wavelength error versus the number of cells per wavelength. The mixed approach shows the biggest wavelength error.

B. Multiresolution Formulations

The dispersion properties of a multiresolution approach will now be examined. Consider a one-dimensional dielectric resonator that is filled with two different dielectrics. According to Maxwell's equations for inhomogeneous media, electric fields are expected to be differentiable smooth on the surface in the center of the cavity, while magnetic fields are not. This problem would lead to a multiresolution algorithm with low order E_x only, but high order H_z.

Choosing $\varepsilon_{r1} = \varepsilon_{r2} = 1$, the following pre-examinations are performed. With all $E_{x_m}^1 = 0$, the system matrix of the eigenvalue problem can be written as

$$\begin{pmatrix} \underline{E}_0 \\ \underline{H}_0 \\ \underline{H}_1 \end{pmatrix} = - \begin{pmatrix} 0 & \frac{C_{00}}{Z_F} & \frac{C_{01}}{Z_F} \\ C_{00} \cdot Z_F & 0 & 0 \\ C_{10} \cdot Z_F & 0 & 0 \end{pmatrix} \begin{pmatrix} \underline{E}_0 \\ \underline{H}_0 \\ \underline{H}_1 \end{pmatrix} \tag{17}$$

leading to the dispersion relationship

$$\det(\boldsymbol{C} - \boldsymbol{I}) = 1 - C_{00}^2 - 2C_{01}C_{10} \stackrel{!}{=} 0. \tag{18}$$

The mixed-order curves are expected to lie between the homogeneous ones. However, in fact, the results are worse than those of zeroth order at any given resolution, as indicated in Fig. 2.

With this prior research, it cannot be anticipated that a multiresolution formulation with higher order H_z in the whole calculation area or just at the surface between the two dielectrics will provide better results than a simple zeroth-order one. Analogous graphs are obtained for Battle–Lemarie families.

TABLE IV
MATERIAL OPERATOR $[\mathcal{E}_S]$ FOR ZEROTH- AND FIRST-ORDER $\mathrm{CDF}(2,2)$ WAVELETS

$m \setminus \tilde{m}$	-1	0	$+1$
$q = 0,\ \tilde{q} = 0$			
-1	ε_{r1}	$\frac{1}{12}(\varepsilon_{r1} - \varepsilon_{r2})$	0
0	0	$\frac{1}{2}(\varepsilon_{r1} + \varepsilon_{r2})$	0
$+1$	0	$\frac{1}{12}(\varepsilon_{r2} - \varepsilon_{r1})$	ε_{r2}
$q = 0,\ \tilde{q} = 1$			
-1	$\frac{1}{24}(\varepsilon_{r2} - \varepsilon_{r1})$	$\frac{1}{24}(\varepsilon_{r2} - \varepsilon_{r1})$	0
0	$\frac{1}{4}(\varepsilon_{r1} - \varepsilon_{r2})$	$\frac{1}{4}(\varepsilon_{r2} - \varepsilon_{r1})$	0
$+1$	$\frac{1}{24}(\varepsilon_{r1} - \varepsilon_{r2})$	$\frac{1}{24}(\varepsilon_{r1} - \varepsilon_{r2})$	0
$q = 1,\ \tilde{q} = 0$			
-1	0	$\frac{1}{6}(\varepsilon_{r1} - \varepsilon_{r2})$	0
0	0	$\frac{1}{6}(\varepsilon_{r2} - \varepsilon_{r1})$	0
$q = 1,\ \tilde{q} = 1$			
-1	$\frac{1}{12}(11\varepsilon_{r1} + \varepsilon_{r2})$	$\frac{1}{12}(\varepsilon_{r2} - \varepsilon_{r1})$	0
0	$\frac{1}{12}(\varepsilon_{r1} - \varepsilon_{r2})$	$\frac{1}{12}(\varepsilon_{r1} + 11\varepsilon_{r2})$	0

IV. CDF(2,2) Boundary Algorithms

A. Dielectric Boundaries

As the stencil size of CDF wavelets exceeds one, exact treatment of dielectric boundaries is only possible with the material operator derived by [1]. For one-dimensional propagation and a dielectric surface located at $y = 0$, this operator reads as

$$D_{x_m}^q(k) = \frac{\varepsilon_0}{\Delta y} \cdot \sum_{\tilde{m}} \sum_{\tilde{q}} [\mathcal{E}_S] \cdot E_{x_{\tilde{m}}}^{\tilde{q}}(k) \tag{19}$$

$$[\mathcal{E}_S] = \varepsilon_{r1} \int_{-\infty}^{0} \tilde{\Psi}_{\tilde{m}}^{\tilde{q}}(y) \Psi_m^q(y) dy + \varepsilon_{r2} \int_{0}^{\infty} \tilde{\Psi}_{\tilde{m}}^{\tilde{q}}(y) \Psi_m^q(y) dy. \tag{20}$$

For $\mathrm{CDF}(2,2)$ wavelets, these integrals have to be calculated numerically making use of the *cascade algorithm* provided by [11]. For 20 iterations, the results are displayed in Table IV. Note that rational fractions replaced the numerical values, being identical in all correct digits. Perhaps they will be shown to be exact by analytical investigations. These results are presented in [6] as well, but their exact quantity is omitted.

Concerning the multiresolution approach, the following field representation was chosen.

1) As the electric field is continuous and differentiable smooth, only zeroth-order coefficients are applied.
2) As the magnetic field is continuous, but not differentiable, one first-order wavelet is arranged in the boundary plane to model the bump [see Fig. 3(a)].

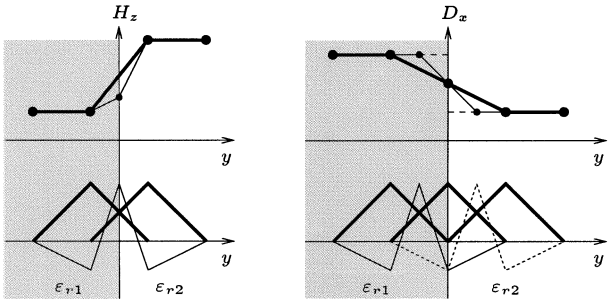

Fig. 3. Modeling of special boundary field curves (top) including zeroth- (thick lines) and first-order (thin lines) wavelets (bottom). (a) Modeling of H_z, (b) Modeling of D_x. The interface between the two dielectric media lies at $y = 0$ (see text for details).

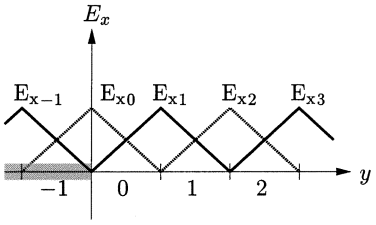

Fig. 4. Tangential electric field in the plane of a thin metallic iris extended up to $y = 0$. To ensure zero tangential field on the iris, wavelet coefficients up to E_{x0} must vanish.

3) As the electric flux jumps, two first order functions are selected to the left and right of the dielectric interface, as shown in Fig. 3(b).

At last, the simplified local sampling approach for $\mathrm{CDF}(2,2)$ wavelets will be observed in the simulations part. Similar to FDTD, this one only uses the main diagonal elements of the first Table IV. Note the equality to zeroth-order Daubechies' wavelets with local sampling, employing the same connection coefficients.

B. Improved $\mathrm{CDF}(2,2)$ *Algorithm for Thin Perfect Electric Conductors (PECs)*

As for other MRTD formulations, PECs have to be modeled in $\mathrm{CDF}(2,2)$ algorithms utilizing the image principle. This applies well for enclosed concave cavities, but yields certain problems when applied to convex edges or thin metallic irises. Especially for the latter, it is easy to improve the performance with a simple change in geometry.

Consider Fig. 4, which shows the x-component of the electric field in a plane parallel to the (x, y)-surface that is half occupied by a thin iris extended up to $y = 0$, but with no limits in the x-direction. For this setup, E_x lies tangential to the PEC and should vanish in the left half-space $(E_x(x, y \leq 0, z = 0) = 0)$. This is usually achieved by adding uneven images in the columns $-1, -2, \ldots$, occupied by the iris while processing the update equations.

For $\mathrm{CDF}(2,2)$, it is not sufficient to apply the image principle only to the negative columns. As Fig. 4 indicates, this procedure leaves the wavelet coefficient E_{x0} untouched, producing nonzero fields on the metallization. A simple extension of the iris by one cell can solve this problem, producing a linear rising

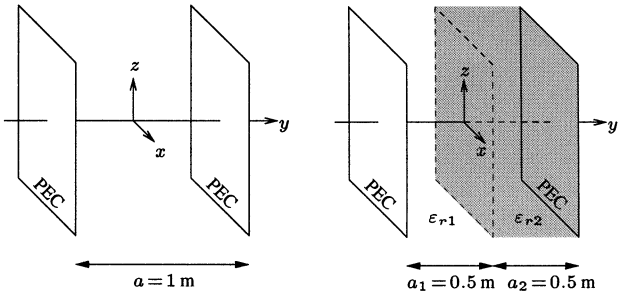

Fig. 5. Two one-dimensional resonators under investigation. (a) Air filled. (b) With dielectric charge.

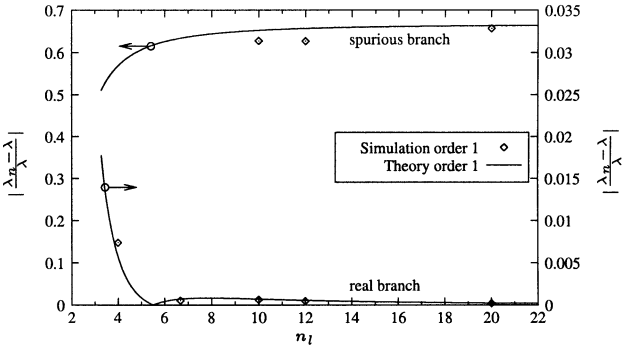

Fig. 6. First-order simulation with spurious modes. Comparison of simulation results and analytically derived wavelength error graphs of Fig. 1.

E_x in front of the edge. Since this evaluation is not straightforward for other field components or wavelet types, it is only possible to talk about an effective aperture height in the MRTD domain, which is supposed to be one cell size larger than the actual geometry in the CDF-MRTD case.

V. Simulations

A. Simulation of Dielectric Boundaries

At first, the air-filled resonator in Fig. 5(a) was analyzed in order to verify the results of Section III. The Courant number was chosen to be $\hat{q} = 0.6$ for FDTD and $\hat{q} = 0.25$ for MRTD. The cells per real wavelength n_l were calculated by resonant order and spatial discretization length Δy for each of the first three resonances, as well as the spurious modes at six and ten overall grid points. Errors in the resonant frequency compared to the trivial analytic case were recalculated to numerical wavelength errors. The results are displayed in Figs. 6 and 7 together with the dispersion graphs.

A good match can be observed for both diagrams. Additional errors are addressed to nonideal boundary positions in the simulation, which cannot be taken into account by the analytical investigation of free-space plane waves.

These results do not encourage higher order attempts. Complete first-order expansions suffer under spurious solutions, what is not bearable for S-parameter extraction. Mixed approaches are worse than one of a complete lower order even in this trivial case so they cannot be expected to be better in general. In [6], results are compared only qualitatively to FDTD with a very high resolution, which does not justify the emphasis of their superiority.

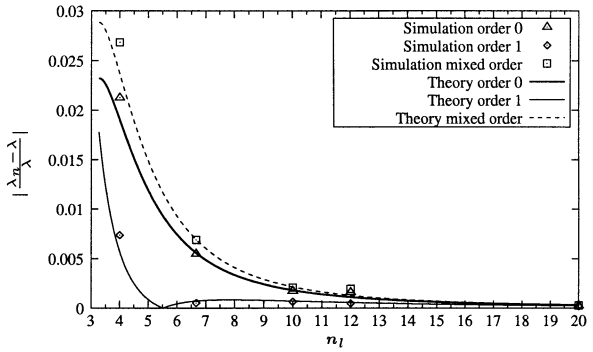

Fig. 7. Mixed-order simulations. Comparison of simulation results and analytically derived wavelength error graphs of Fig. 2.

TABLE V
NUMERICAL RESULTS FOR THE CHARGED RESONATOR. THE ANALYTIC RESONANT FREQUENCY OF THE DOMINANT MODE IS 59.82 MHz

total cells	FDTD	CDF(2,2)		
		loc. samp.	[$\mathcal{E}$] order 0	multires.
6	59.38 (-0.736%)	60.40 (+0.970%)	60.05 (+0.384%)	64.38 (+7.623%)
10	59.69 (-0.217%)	60.03 (+0.351%)	59.87 (+0.084%)	62.33 (+4.196%)

The next study dealt with a dielectrically charged resonator utilizing different boundary algorithms for $\mathrm{CDF}(2,2)$ wavelets. Having maximum fields in the middle of the cavity close to the boundary, the basic resonant mode is the most interesting one. Simulation parameters were as before, and the step in the dielectric permittivity was chosen to be $\varepsilon_{r1} : \varepsilon_{r2} = 1 : 10$ in order to obtain spatially strong varying fields at the interface. Results for the dominant mode are displayed in Table V.

The most striking aspect are the poor results for the multiresolution column. They are far worse than those of any other technique and improve only by adding wavelets of higher order to each field component in every cell. This strongly supports the idea of partially higher order approaches yielding worse results compared to uniform lower order ones because of the truncated field expansion that was put up in the analytic examination in Section III.

Even the local sampling approach used in many publications so far (e.g., [3], [5] and [8]) cannot hold against FDTD of the same resolution. Note that the algorithm for $\mathrm{CDF}(2,2)$ wavelets in zero order with local sampling is identical to the one with compactly supported Daubechies' wavelets.

Only the accurate treatment using the material operator in its complete form can justify a cell reduction compared to FDTD by a factor of 1.5 to 2.

B. Simulation of PECs

In order to test the modeling of PECs, different resonating three-dimensional cavities have been studied with MRTD and compared to the results of conventional FDTD. The Courant numbers were chosen to be $\hat{q} = 0.57$ at the stability limit for FDTD and $\hat{q} = 0.1$ for MRTD simulations.

The ordinary rectangular resonator in Fig. 8(a) has been the target of several successful examinations with MRTD in the past

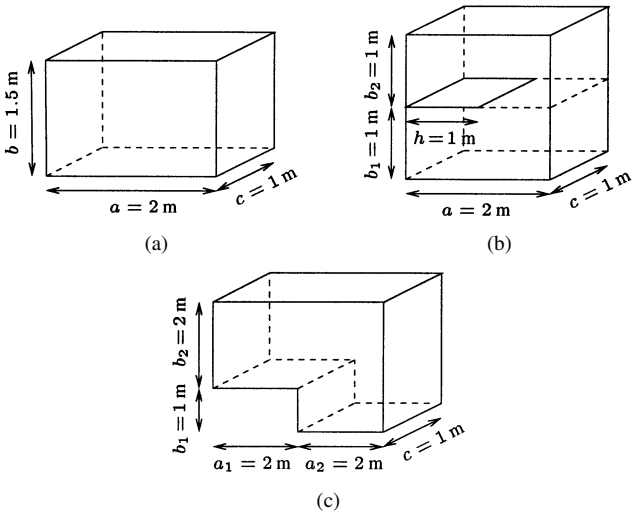

Fig. 8. Different resonating cavities bounded by PECs. (a) Rectangular. (b) With thin iris. (c) L-shaped.

TABLE VI
DOMINANT RESONANT FREQUENCY OF CAVITY 8(a). THE ANALYTICAL VALUE IS 124.91 MHz

cells per m	FDTD	CDF(2,2)	Battle-Lemarie
2	122.98 (-1.545%)	125.40 (+0.392%)	124.98 (+0.056%)
4	124.45 (-0.368%)	124.96 (+0.040%)	
6	124.66 (-0.200%)	124.93 (+0.016%)	
12	124.86 (-0.040%)		

(e.g., [1], [2], and [4]). Its results in Table VI were added here just for the sake of completeness.

Even with very low discretization rates, smooth MRTD approaches are capable of modeling the exclusively harmonic spatial field distributions with negligible phase error, as predicted in all analytical investigations.

The next cavity under investigation has a thin iris located at its center in order to test the modified PEC algorithm of Section IV-B with the proposed effective aperture height. Again, the basic resonant mode is of primary interest due to high field amplitudes in the iris' plane and, thus, a strong dependence on the metallization height. Modes with central nodes are not affected by the iris' dimensions and, therefore, error magnitudes are in line with those of the rectangular cavity for all schemes.

Results for this dominant resonant frequency are given in Table VII for three different discretization rates.

Again, a reduction of nodes per wavelength by a factor of three or more is possible. Note that the first CDF value has not converged yet and that no edge corrections have been applied to conventional FDTD.

Unfortunately, this geometry adjustment cannot be extended to arbitrary forms, leading to poor results for MRTD schemes on outer edges. A simple but striking example is the L-shaped cavity in Fig. 8(c). The basic mode was chosen for examination according to the same argumentation as before, with the results displayed in Table VIII.

TABLE VII
DOMINANT RESONANT FREQUENCY OF CAVITY 8(c). THE MODE-MATCHING TECHNIQUE AND SPECTRAL-DOMAIN APPROACH VALUE IS 137.90 MHz

cells per m	FDTD	CDF(2,2)	Battle-Lemarie
2	104.79 (-24.01%)	139.77 (+1.356%)	108.30 (-21.46%)
4	119.01 (-13.70%)	135.06 (-2.059%)	120.58 (-12.56%)
8	127.97 (-7.201%)	135.94 (-1.421%)	128.88 (-6.541%)

TABLE VIII
DOMINANT RESONANT FREQUENCY OF CAVITY 8(c). THE MMT VALUE IS 76.04 MHz

cells per m	FDTD	CDF(2,2)	Battle-Lemarie
2	76.61 (+0.750%)	78.18 (+2.814%)	78.09 (+2.696%)
3	76.49 (+0.598%)	77.24 (+1.578%)	77.23 (+1.565%)
4	76.36 (+0.421%)	76.84 (+1.052%)	76.93 (+1.170%)

Due to the systematic error of the image principle in front of the edge, MRTD failures even exceed those of conventional FDTD with the same discretization rates.

VI. CONCLUSION

In the first part of this paper, MRTD schemes with local addition of higher order wavelets have been investigated. Reasons against these multiresolution approaches were found in analytical studies, as well as in simulations on resonant structures. In both cases, they lead to less accurate results. All acquired points contradicting the fixed use of different wavelet orders in one mesh are as follows.

1) Partially higher order approaches seem to yield worse results than a uniform lower order one due to truncated field expansion.
2) As in FDTD, it is not possible to formulate a general stability criterion for multigrid approaches since MRTD's maximum Courant number strongly depends on the wavelet level [4].
3) Above the zeroth-order scheme, spurious solutions must be expected.
4) According to [12], the shift of dual subgrids for E- and H-fields is a function of the wavelet level in homogeneous schemes in order to obtain minimal dispersion. This is not possible for spatially varying field expansions.
5) Haar wavelets do not allow multiresolution at all since different levels do not couple (see Table I and [13]).

Therefore, an *a priori* multiresolution approach is not thought to be of any advantage over zeroth-order calculations. Future work should concentrate on dynamic scale adaption [7].

Additionally, it was shown that CDF or Daubechies' wavelets with a local sampling technique to model dielectric boundaries are inferior to conventional FDTD formulations with the same resolution even at simple one-dimensional structures. This effect is expected to increase in the three-dimensional case with jumping normal field components, as their approximation with smooth wavelets is worse compared to hard jumping FDTD rectangles.

In the second part of this paper, studies focused on infinitely thin perfect electric walls. Due to the noncompact triangular form of CDF dual wavelets, these thin metallizations can be modeled more precisely by simply enlarging the iris length by one cell. Unfortunately, this proceeding cannot be transferred to any edge form.

Both conclusions show that CDF-MRTD algorithms seem to be superior over FDTD only for certain geometries such as ideal microstrip lines with infinitely thin metallizations and uncomplicated dielectric arrangements. Since these compositions are candidates for spectral-domain methods, MRTD must be compared to those for propositions about computational time and memory.

REFERENCES

[1] M. Krumpholz and L. P. B. Katehi, "MRTD: New time-domain schemes based on multiresolution analysis," *IEEE Trans. Microwave Theory Tech.*, vol. 44, pp. 555–571, Apr. 1996.

[2] M. Fujii and W. J. R. Hoefer, "A three-dimensional Haar-wavelet-based multiresolution analysis similar to the FDTD method-derivation and application," *IEEE Trans. Microwave Theory Tech.*, vol. 46, pp. 2463–2475, Dec. 1998.

[3] M. Werthen and I. Wolff, "A novel wavelet based time domain simulation approach," *IEEE Microwave Guided Wave Lett.*, vol. 6, pp. 438–440, Dec. 1996.

[4] T. Dogaru and L. Carin, "Multiresolution time-domain using CDF biorthogonal wavelets," *IEEE Trans. Microwave Theory Tech.*, vol. 49, pp. 902–912, May 2001.

[5] M. Fujii and W. J. R. Hoefer, "Time-domain wavelet Galerkin modeling of two-dimensional electrically large dielectric waveguides," *IEEE Trans. Microwave Theory Tech.*, vol. 49, pp. 886–892, May 2001.

[6] T. Dogaru and L. Carin, "Scattering analysis by the multiresolution time-domain method using compactly supported wavelet systems," *IEEE Trans. Microwave Theory Tech.*, vol. 50, pp. 1752–1760, July 2002.

[7] E. M. Tentzeris, A. Cangellaris, L. P. B. Katehi, and J. Harvey, "Multiresolution time-domain (MRTD) adaptive schemes using arbitrary resolutions of wavelets," *IEEE Trans. Microwave Theory Tech.*, vol. 50, pp. 501–515, Feb. 2002.

[8] Y. W. Cheong, Y. M. Lee, K. H. Ra, J. G. Kang, and C. C. Shin, "Wavelet-Galerkin scheme of time-dependent inhomogeneous electromagnetic problems," *IEEE Microwave Guided Wave Lett.*, vol. 9, pp. 297–299, Aug. 1999.

[9] Q. Cao, Y. Chen, and R. Mittra, "Multiple image technique (MIT) and anisotropic perfectly matched layer (APML) in implementation of MRTD scheme for boundary truncations of microwave structures," *IEEE Trans. Microwave Theory Tech.*, vol. 50, pp. 1578–1589, June 2002.

[10] E. M. Tentzeris, R. L. Robertson, J. F. Harvey, and L. P. B. Katehi, "Stability and dispersion analysis of Battle–Lemarie-based MRTD schemes," *IEEE Trans. Microwave Theory Tech.*, vol. 47, pp. 1004–1012, July 1999.

[11] I. Daubechies, *Ten Lectures on Wavelets*. Philadelphia, PA: SIAM, 1992.

[12] C. D. Sarris and L. P. B. Katehi, "Fundamental gridding related dispersion effects in multiresolutional time domain schemes," *IEEE Trans. Microwave Theory Tech.*, vol. 49, pp. 2248–2257, Dec. 2001.

[13] S. Grivet-Talocia, "On the accuracy of Haar-based multiresolution time-domain schemes," *IEEE Microwave Guided Wave Lett.*, vol. 10, pp. 397–399, Oct. 2000.

Martin Peschke received the Dipl.-Ing. degree from the University of Ulm, Ulm, Germany, in 2002, and is currently working toward the Dr.-Ing. degree in optoelectronics at the University of Ulm.

His areas of interest are electromagnetic-wave theory, computational electrodynamics, and integrated optics.

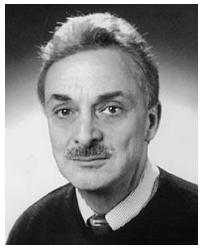

Wolfgang Menzel (M'89–SM'90–F'01) received the Dipl.-Ing. degree in electrical engineering from the Technical University of Aachen, Aachen, Germany, in 1974, and the Dr.-Ing. degree from the University of Duisburg, Duisburg, Germany, in 1977.

From 1979 to 1989, he was with the Millimeter-Wave Department, AEG, Ulm, Germany [now the European Aerospace, Defense, and Space Systems, (EADS)]. From 1980 to 1985, he was Head of the Laboratory for Integrated Millimeter-Wave Circuits. From 1985 to 1989, he was Head of the entire Millimeter-Wave Department. During that time, his areas of interest included planar integrated circuits (mainly on the basis of fine-line techniques), planar antennas, and systems in the millimeter-wave frequency range. In 1989, he became a Full Professor with the University of Ulm, Ulm, Germany. His current areas of interest are multilayer planar circuits, waveguide filters and components, antennas, millimeter-wave and microwave interconnects and packaging, and millimeter-wave application and system aspects.

Dr. Menzel is currently an associate editor for the IEEE TRANSACTIONS ON MICROWAVE THEORY AND TECHNIQUES. From 1997 to 1999, he was a Distinguished Microwave Lecturer for Microwave/Millimeter Wave Packaging. From 1997 to 2001, he chaired the German IEEE Microwave Theory and Techniques (MTT)/Antennas and Propagation (AP) Chapter.